Tracing, Amplifying, and Steering Chromophore-Bath Coherences by Ultrashort Pulse Trains

Heide Ibrahim, Mónika Héjjas, and Nikolaus Schwentner*

Institut für Experimentalphysik, Freie Universität Berlin, Arnimallee 14, D-14195 Berlin, Germany

(Received 15 April 2008; published 24 February 2009)

With a train of 5 phase controlled ultrashort pulses, we enhance a coherent vibronic transition to exceed a dominant incoherent background. The interference in the chromophore generates a spectral comb which is adjusted to a progression of internal Br_2 vibrations coupled to phonons of the surrounding Ar lattice. It steers the mode-specific phase evolution of the system. The trains are generated by straightforward programing of the spectral comb in a pulse shaper unit. Excitations involving several hundred degrees of freedom remain coherent on a picosecond time scale.

DOI: 10.1103/PhysRevLett.102.088301 PACS numbers: 82.53.−k, 63.20.−e

Coherent control scenarios are extensively explored in relation to quantum computing and manipulation of photochemical reactions [1,2]. Their application requires the extension from a few to many degrees of freedom, which goes along with an increasing tendency to decoherence. Electronic decoherence times on the order of 100 fs are expected for chromophores in the condensed phase, which represents a severe challenge [3]. However, quantum interferences from double pulse excitation were already observed for exciplexes on He nanodroplets [4] and molecules in matrices [5]. We go even further and demonstrate multiple pulse interferences from excitation with trains of several coherent pulses. They require long lasting electronic coherences on the order of picoseconds for the chosen chromophore-bath system Br_2:Ar, where Br_2 molecules act as chromophores in a surrounding fcc-structured Ar crystal. Constructive interference results in a progressive enhancement of selected wave packet amplitudes in the coherent part of the system. We demonstrate that vibronic coherences in the electronically excited B state [Fig. 1(b)] can be strongly amplified in this way. In absorption spectra [Fig. 2(a)], the faint B state features are buried in an overwhelming continuous background which originates from the A state excited above its gas phase dissociation limit and bound only by the matrix cage [6]. Therefore, the A state dynamics dominates in single pulse time resolved pump-probe experiments. It will be shown that with the coherent pulse train excitations we achieve B state wave packet amplitudes which exceed the A state ones considerably. The amplification is so efficient that even weak sidebands of the B state lines [Fig. 1(a)] stemming from a combined excitation of Br_2 vibration and matrix phonons can be addressed coherently. We apply a novel and straightforward approach for pulse train generation that has advantages compared to the more widespread variants of coherent control. It avoids the intermediate steps necessary for an analytical programing of pulse sequences [7] and does not require a selection of tasks, like in optimal control with closed feedback loops [3]. In a first step, we determined by high resolution spectroscopy the faint B state signatures [6] shown in Figs. 2(a) and 2(b). Then we program them directly into the pixels of a liquid crystal display (LCD) that is the active device in a typical pulse shaper unit with $4f$ optics and gratings [2]. This pure amplitude filtering generates pulse trains whose temporal amplitude and phase distributions reproduce in the wave packet interferogram the specific details of vibrational energy shifts due to anharmonicity, avoided crossings, and phonon modes [6].

Each subpulse in the train is short (≈40 fs) with respect to the pulse separation in the train (250 fs) and has the same structureless spectral envelope as shown by the solid line in Fig. 2(c). Thus, all individual pulses would prepare similar wave packets from a coherent superposition of vibrational and phonon eigenstates. However, the amplitude and phase information remains stored in the coherent part of the excited chromophore-bath entity. There, the interference of already oscillating wave packets with the new ones produces spectral combs [dashed line in Fig. 2(c)]. The comb spacing is determined by the inverse pulse separation and the spectral position under the envelope (solid line) by the phase relation among the pulses. The width of the teeth

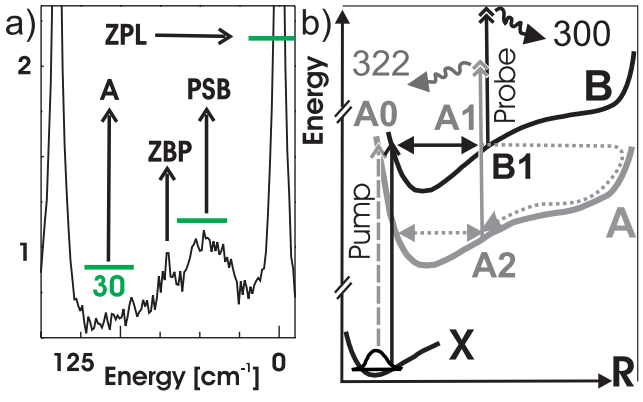

FIG. 1 (color online). (a) Zoom into a PSB with an indicated resolution of 30 cm^{-1}; see Fig. 2(b) and text. (b) Energy scheme with ground state X and covalent states A (solid gray line) and B (solid black line). For $A0$–2, $B1$, and probe arrows, see text.

shrinks with the number of coherently accepted pulses. This requires that during the train duration (5 pulses, 1.2 ps) the chosen carrier and entity phase relation stays stable. These spectral properties of the wave packet interferogram are analogous to the evolution of the spatial pattern in going from single- to multislit interferences. Both cases obey similar Fourier transformations, and analytic expressions are treated in [8]. Such combs were proposed for sharp spectral selection in isolated cold systems [9]; here we apply them to control a complex chromophore-bath interaction with adapted resolution. We steer the phonon content by shifting the spectral position of the comb via the phase distribution in the pulses of the train until it matches the spectroscopic features and demonstrate that phonons excited with the first members in the train can be extinguished by the following pulses via destructive interference.

Dihalogens in rare gas matrices have proven to be flexible building bricks for investigating chromophore-lattice interactions [10,11]. Br_2 in solid Ar matrices was chosen because of tested conditions for pump-probe spectroscopy [12], the theoretical background [13,14], and the resolved zero phonon lines (ZPLs) and phonon sidebands (PSBs). In this favorable case, it is possible to extract the pure B contribution by spectral selection [6] as shown in Fig. 2(b). The faint features correspond to the sharp vibrational progression of ZPLs with a FWHM linewidth of 3–4 cm^{-1} and a lifetime of about 1.5 ps. Each represents an exclusive excitation of an intramolecular Br_2 mode. Every ZPL is accompanied on the blue side by a broad PSB extending up to 80 cm^{-1} [Fig. 1(a)]. It corresponds to a simultaneous excitation of chromophore and phonon modes of the environment.

Mixtures of 1:500 Br_2:Ar are deposited in UHV on a cooled window in a standard way [12] and investigated at 6 K. A commercial 1 kHz Ti:sapphire regenerative amplifier pumps a noncollinear optical parametric amplifier tuned to 590 nm. The pump beam passes the pulse shaper (see introduction), and the resulting pulse trains are characterized with respect to time structure by X-FROG [15]. With the pulse shaper we write a sharp progression of ZPLs [dashed line in Fig. 2(c)] or PSBs [Fig. 2(b)] into the spectral distribution to generate the pulse trains. The probe beam passes a delay stage, and both beams are superimposed on the sample. Laser-induced fluorescence (LiF) from charge transfer states [Fig. 1(b)] with bands at 322 and 300 nm is collected, dispersed in a monochromator, and recorded by a photomultiplier and boxcar integrator. Intensities are given in arbitrary units due to uncalibrated detection sensitivity. Only a small fraction of about 10^{-4} of the molecules is excited with a pulse energy of 0.1 μJ (diameter 50 μm) due to the small cross section of 2×10^{-20} cm^2 at 590 nm [6].

An unshaped single pulse centered at 590 nm with the spectral width like in Fig. 2(c) results in a pump-probe

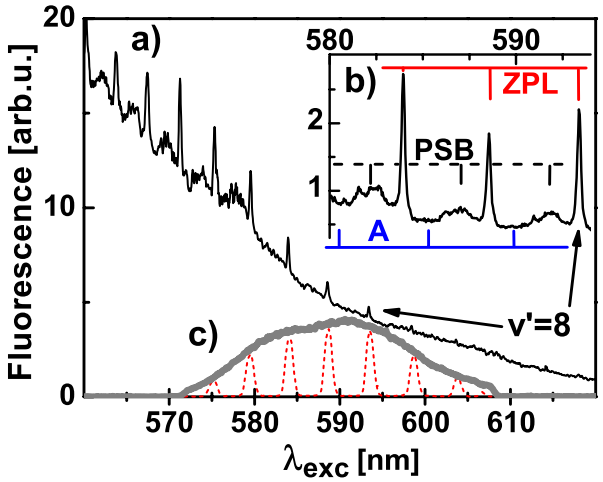

FIG. 2 (color online). (a) Spectrum representing the absorption of Br_2:Ar (Ref. [6]). (b) Zoom into selected B state excitation spectrum with spectral positions for the frequency comb A, ZPL, and PSB starting from $B(v' = 8)$. (c) Frequency comb matching the B contributions (dashed line) and envelope of a single pulse (solid gray line).

spectrum for 322 nm emission shown in Fig. 3(a) which can be explained in the following way: A wave packet is generated in the $A\,^3\Pi_{1u}$ state via the $A \leftarrow X$ transition [Fig. 1(b)]. From the Franck-Condon (FC) window at $A0$, it propagates towards the outer turning point in the dashed trajectory. In the gas phase it would start with energy above the dissociation threshold and never return. In the matrix the internuclear distance R between the two Br atoms expands until they bump into the cage atoms in a well-defined geometry [12]. In this collision they transfer most of their kinetic energy to the cage and do not return to the initial FC region, but rather deep in the A state potential where they start to oscillate nearly undistorted [16]. For these conditions the A state wave packet is recorded with high efficiency at time delays which correspond to the passage times at $A1$ and $A2$, indicated in Fig. 1(b). Simultaneous to $A0$, the pump pulse prepares a wave packet in the B state which is probed two-photonically at $B1$, close to the outer turning point as indicated by the full double arrow. The wave packet is located deep in the B state potential well. Therefore, it feels little interaction with the cage and oscillates with nearly the gas phase period ($\approx$250 fs) with marginal decoherence passing the initial FC region with every period. $B1$ is merged with $A1$; however, the second passage of the wave packet at $B2$ is isolated and clearly visible. Because of electronic transition strengths and FC factors, the $B2$ amplitude in Fig. 3(a) is about 10 times lower than the $A1$ amplitude.

Next, we generate a pulse train by directly writing the detailed experimental ZPL spectral structure [6] on the LCD transmission with an open width of 30 cm^{-1} [Fig. 1(a)]. The average spacing in the progression corresponds to 130 cm^{-1}, and the intensity is reduced by a

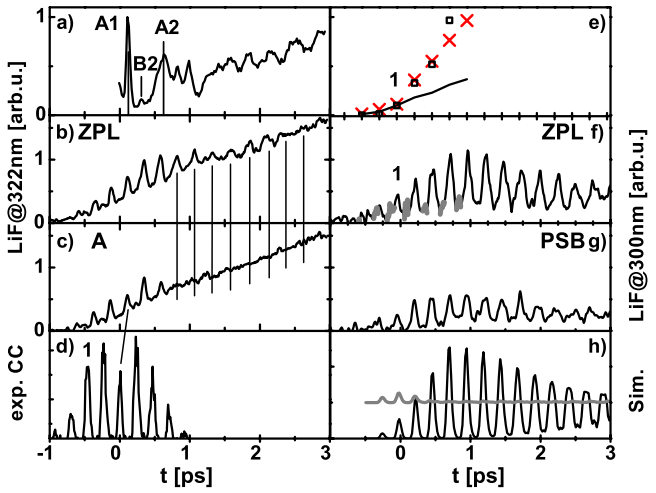

FIG. 3 (color online). LiF recorded at (a)–(c) 322 and (f), (g) 300 nm. (a) Single excitation pulse experiment. (b) Excitation with ZPL comb pulse train [Figs. 2(b) and 2(c)] (c) with comb in position A; (b),(c) on the same scale, (a) multiplied by 0.5. (d) Measured intensity cross correlation of the pulse train with the probe pulse used in (b)–(g). The first strong pulse is indicated by "1." (e) Integrated peak intensity from (f) (crosses), compared with accumulated linear (line) and squared (open squares) pulse intensities from (d). The line and the squares are normalized for the first strong peak 1. (f) ZPL excitation like in (b), with contributions from the B state (black line) and the A state (small gray parts). (g) PSB comb excitation; (f),(g) on the same scale. (h) Simulation for constructive (black) and destructive B excitation (gray line).

factor of 4. The train [shown in Fig. 3(d)] follows the B period of 250 fs, the envelope of 1.2 ps is determined by the spectral resolution in the shaper (30 cm^{-1}), and the width of each subpulse of 70 fs in the cross correlation corresponds to a pulse duration of 40 fs. The resulting pump-probe spectrum in Fig. 3(b) is now dominated by the B state dynamics, pointed out by the vertical lines. After pulse termination any A dynamics are hardly discernible, while the monotonically rising background is a leftover from A. Thus, the goal of enhancing B relative to A is fully reached, due to coherent vs incoherent superposition, treated next.

We shift the programmed spectral comb to the A positions of Fig. 2(b). The condition for interference is reduced to the small spectral range between the termination of PSB and the next ZPL where only an A contribution is expected. We observe in Fig. 3(c) a smoothly rising background from accumulated incoherent A parts recorded like in (b). The dynamical part in (c) is just a linear copy of the pulse train shown in (d) as the measured cross correlation intensity of the pump sequence with the probe pulse. Each one of the 40 fs pulses in the train generates an A wave packet. It is seen only once in passing $A1$ with an intensity proportional to the subpulse intensity which is reduced compared to Fig. 3(a) by about a factor of 20 due to the splitting in several subpulses [Fig. 3(d)] and the shaper transmission. The pulse sequence is centered around $t = 0$, and even the drop there is reproduced in (c). This proves the incoherent accumulation of A with a single dynamic detection.

Now we turn back to constructive interference of B state wave packets and resort to 300 nm LiF in (f). Here, the probe window $A2$ is not open due to insufficient probe photon energy; thus, we suppress the monotonically increasing A contributions. With the ZPL comb we observe a progressive increase in the B signal with the number of accumulated pulses. The 5 central pulses in (d) have rather similar intensities. For N equal pulses, the coherent signal would rise with N^2 [8] in agreement with the measured black line in (f). To demonstrate the nonlinear increase, we display the area of each one of the first seven oscillations of (f) by crosses in (e). They follow the accumulated squared intensity of the pulse train (squares) very well and thus rise much stronger than the linear accumulation (line). Depopulation, especially by predissociation as observed in [6], causes a lower intensity of the last two points in (e). In between the enhanced B state dynamics in (f), tiny A state wave packets of equal heights show up (thick gray parts), which pass $A1$ only once and do not accumulate because of a mismatch in timing and of energy relaxation [as discussed in Fig. 3(c)].

To simulate the coherent B dynamics for constructive and destructive interference for pulse trains [black and gray line in (h), respectively], we adapted a published code [17,18] which treats excitation of wave packets in first-order perturbation theory and their quantum mechanical propagation. We include experimental X and B state parameters [6] and appropriate probe window conditions but no depopulation and decoherence. The black line in (h) shows the simulated result for the ZPL configuration, and the agreement with experiment in (f) is very convincing.

Finally, we record the 300 nm LiF for the programmed PSB comb [Fig. 2(b)] as depicted in Fig. 3(g). We observe once more a progressive increase in the beginning. The intensity stays, however, constant after the center of the pulse sequence, and the final signal is lower by a factor of 2–2.5 compared to (b), which is explained now. After coherent superposition of the full pulse train, the spectral sharpness of the frequency comb covers the full ZPL, and even the most stringent interference of the last pulses does not cut into it [Fig. 1(a)]. This is different for the broad PSB. Thus, the destructive part of the interference conditions cuts more and more of the PSB, and the progressive constructive part has to compensate for this loss. The spectral weight of the PSB included within the chosen bandwidth of 30 cm^{-1} is about half of that of the ZPL. If we multiply the plot of Fig. 3(g) with these weight factors, we come close to the coherent result in (f). This consideration shows the lasting coherence properties of the PSB.

To emphasize the coherence even throughout the whole PSB, we turn back to excitation in the A position

in Fig. 3(c). The pulse train power spectra for all three excitation positions ZPL, PSB, and A [Fig. 2(b)] are identical to Fig. 3(d), and only the phases determine the selection of the favored comb position by interference. Every pulse with its 40 fs duration covers the full spectrum [Fig. 2(c)], and in an incoherent accumulation with statistical phase we would observe B wave packets linearly increasing with deposited intensity. The long lasting vibrational coherence in B would preserve this contribution also at long times. There is, however, no discernible B contribution in Fig. 3(c), and this can be explained only by a destructive interference of new wave packets with the former ones in B. The destructive interference with the full phonon contribution (ZPL and PSB) requires that also PSB wave packets preserve the phase memory for several round trips. The gray line in (h) shows the result of the simulation for the pulse sequence at comb position A (an offset is added for better visibility). The first pulses generate some population in B. However, the more pulses are added the more efficiently population is depleted because destructive interference becomes more stringent. At the termination of the pulse train, no discernible population survives, in full agreement with the experiment in (c). This emphasizes the high phase stability for ZPL and PSB wave packets. For ZPL it is consistent with the narrow spectral width yielding a lifetime of 1.5 ps, while a conversion of the full PSB would correspond to about 100 fs. Obviously, the PSB represents a distribution of phonon modes with long living individual components.

Phonons originate from an expanding electronic wave function in the $B \leftarrow X$ transition [displacive excitation of coherent phonons (DECP)], and also the intramolecular vibrations couple to the matrix, according to the spectroscopic evidence. Initially, normal modes which display the local symmetry of this point defect are excited [13], and finally they decay into bulk phonon modes of the fcc Ar crystal. The PSB shape resembles the Ar phonon density of states [6], and the maximum around 70 cm^{-1} in Fig. 1(a) can be attributed to the zone boundary phonon (ZBP) [19]. Scrambling within the phonon modes and even only a propagation of the phonon part in the excitation from the chromophore into the surrounding bulk changes the transition energy and would thus destroy the electronic coherence observed in the phase sensitive pulse train accumulation. Coherent ZBPs coupled for several picoseconds to the chromophore were observed in the DECP process, and the weak damping was attributed to its vanishing group velocity [19]. For the PSB comb [Fig. 2(b)] we cut out a 30 cm^{-1} broad band in the middle part around 40 cm^{-1} shown in Fig. 1(a). It is remarkable that electronic and vibrational coherence extend into the picosecond regime also for all of those modes being resonant with delocalized matrix phonons. For this range of the phonon dispersion curve, the sound velocity is 10–15 Å/ps. The phonon amplitudes should spread out in 1 ps over several shells containing several hundred neighboring atoms as predicted also by classical trajectory calculations [20]. The extinction of B state contributions in Fig. 3(c) by destructive interference for excitation in the A comb situation indicates, however, that the major part of the phonon modes preserves electronic coherence during the full pulse sequence. Calculations are typically carried out for boxes which include one or two shells of matrix atoms. Thus, the predicted coherent control of photochemistry [13] relies on the coherence for which we give an experimental proof. A theoretical modeling of the coupling to the bath has still to be provided [13].

We thank Dr. M. Gühr, Dr. M. Fushitani, Dr. A. Borowski, Professor O. Kühn, and Professor J. Manz for intense discussions and the DFG with SFB 450 for financial support.

*nikolaus.schwentner@physik.fu-berlin.de

[1] Special issue on Coherent Control [J. Phys. B **41**, 7 (2008)].
[2] P. Nuernberger, G. Vogt, T. Brixner, and G. Gerber, Phys. Chem. Chem. Phys. **9**, 2470 (2007).
[3] M. P. A. Branderhorst *et al.*, Science **320**, 638 (2008).
[4] M. Mudrich *et al.*, Phys. Rev. Lett. **100**, 023401 (2008).
[5] M. Fushitani, M. Bargheer, M. Gühr, and N. Schwentner, Phys. Chem. Chem. Phys. **7**, 3143 (2005).
[6] H. Ibrahim, M. Gühr, and N. Schwentner, J. Chem. Phys. **128**, 064504 (2008).
[7] J. Hauer, H. Skenderovic, K.-L. Kompa, and M. Motzkus, Chem. Phys. Lett. **421**, 523 (2006).
[8] S. Mukamel, *Principles of Nonlinear Optical Spectroscopy* (Oxford University Press, New York, 1995).
[9] A. Peer, E. A. Shapiro, M. C. Stowe, M. Shapiro, and J. Ye, Phys. Rev. Lett. **98**, 113004 (2007).
[10] M. Gühr, M. Bargheer, and N. Schwentner, Phys. Rev. Lett. **91**, 085504 (2003).
[11] M. Ovchinnikov and V. A. Apkarian, J. Chem. Phys. **108**, 2277 (1998).
[12] M. Gühr *et al.*, Phys. Chem. Chem. Phys. **9**, 779 (2007).
[13] A. Borowski and O. Kühn, Chem. Phys. **347**, 523 (2008).
[14] A. Borowski and O. Kühn, J. Photochem. Photobiol., A **190**, 169 (2007).
[15] S. Linden, H. Giessen, and J. Kuhl, Phys. Status Solidi B **206**, 119 (1998).
[16] H. Ibrahim, Ph.D. thesis, Freie Universität Berlin, 2008.
[17] D. Tannor, http://www.weizmann.ac.il/chemphys/tannor/home.html.
[18] M. Gühr, H. Ibrahim, and N. Schwentner, Phys. Chem. Chem. Phys. **6**, 5353 (2004).
[19] M. Gühr and N. Schwentner, Phys. Chem. Chem. Phys. **7**, 760 (2005).
[20] T. Kiljunen, M. Bargheer, M. Gühr, and N. Schwentner, Phys. Chem. Chem. Phys. **6**, 2185 (2004).